

Synchrotron x-ray studies of vitreous SiO₂ over Si(001). I. Anisotropic glass contributionM. Castro-Colin,¹ W. Donner,¹ S. C. Moss,^{1,2} Z. Islam,³ S. K. Sinha,⁴ R. Nemanich,⁵
H. T. Metzger,⁶ P. Bösecke,⁶ and T. Shillli⁶¹*Physics Department, University of Houston, Houston, Texas 77204-5005, USA*²*Texas Center for Superconductivity and Advanced Materials, University of Houston, Houston, Texas 77204, USA*³*Advanced Photon Source, Argonne National Laboratory, Argonne, Illinois 60439, USA*⁴*Department of Physics, University of California San Diego, California 92093-0354, USA*⁵*Department of Physics, North Carolina State University, Raleigh, North Carolina 27695, USA*⁶*European Synchrotron Radiation Facility, BP 220, 38043 Grenoble CEDEX 9, France*

(Received 9 July 2004; published 13 January 2005)

While numerous investigations of the structure and interface of amorphous SiO₂ thermally grown on Si, theoretical as well as experimental, have been carried out over the years, a definitive picture of this thin gate oxide and its interface remains lacking. We have explored this issue using synchrotron x rays in grazing incidence geometry. In this geometry a fourfold modulation in the first sharp diffraction peak (FSDP) from thin vitreous SiO₂ of 100 and 500 Å thickness can be observed. While the FSDP exhibits a modulation throughout the entire film, this modulation decays away from the interface. Reflectivity measurements were also performed, which reveal an interfacial layer of 3% density increase in the SiO₂ film over the bulk (film) density.

DOI: 10.1103/PhysRevB.71.045310

PACS number(s): 68.47.Gh, 61.10.Eq, 61.43.Fs, 78.70.Ck

I. INTRODUCTION

For the sake of clarity, we have decided to present the results and analyses carried out in consecutive papers. The first (present paper) contains an analysis of the amorphous phase of the films, together with reflectivity measurements that complement the data discussed. In the second paper,⁵² a crystalline component detected by means of crystal truncation rod analysis, as well as its corresponding modeling, is included. It is also in the second paper where we attempt to combine all findings into a plausible paradigm for the structure.

Thermally grown amorphous SiO₂ on crystalline Si has served as the gate oxide in complementary metal oxide semiconductor (CMOS) processing due to several key features, including stability, high SiO₂-Si interface quality, and electrical isolation properties.¹ The continuous thinning of the gate oxide has exhibited features that degrade its performance,² and this has driven a series of efforts to deepen the knowledge of this system. In particular, the interface between crystalline Si and amorphous SiO₂ has received special attention. Studies have used experimental techniques such as medium-ion-energy spectroscopy,³ electron-energy-loss spectroscopy (EELS),⁴ x-ray-photoelectron spectroscopy (XPS),^{5,6} transmission electron microscopy,⁷ and ion scattering,¹¹ among many others, together with various theoretical investigations.⁸⁻¹² In spite of the extensive research, the nature of this SiO₂ layer requires a detailed understanding, not only because of its technological impact, but also because amorphous SiO₂ is classically understood as a continuous random network (CRN) glass.¹³ In this case interest arises regarding the interface morphology and its relation to the degree of order present throughout the expectedly amorphous film, when it is in contact with its crystalline silicon substrate.

II. AMORPHOUS NATURE OF SiO₂

Traditionally, amorphous or glassy materials are identified as a frozen liquid,¹⁴⁻¹⁹ and liquids (together with gases) do not possess the translational symmetry of crystalline materials. Although translational symmetry, or long-range order (LRO), is absent, it is well known that concepts of medium-range order (MRO) and short-range order (SRO) can still aid in the characterization of structure within amorphous solids.

In vitreous SiO₂, tetrahedra of oxygen (O) atoms surround silicon (Si) atoms, as in Fig. 1, to yield a basic SiO₄ unit. Thus the SiO₄ tetrahedra share corners with each other such that an O atom is linked to two Si atoms. Moreover, the relative orientation of these tetrahedra vary within wide enough limits,²⁰⁻²⁵ to preclude any crystalline interpretation. We should recall that SRO describes the nearest-neighbor bonding environment of Si and O, and that MRO involves the specification of the dihedral²⁶ and intertetrahedral $\theta(\text{Si-O-Si})$ ($\approx 148^\circ$, Refs. 25, 27, and 28) bond angles, along with other features such as ring statistics.²¹

A prominent feature of the well-known structure factor in amorphous materials is the first sharp diffraction peak (FSDP), as displayed in Fig. 1, whose interpretation has received a great deal of attention.^{27,29-34} In reciprocal space, for amorphous SiO₂, the FSDP appears at $Q_p \approx 1.5 \text{ \AA}^{-1}$. From the point of view of Fourier analysis, it can reasonably be said that it corresponds to a period given by $2\pi/Q_p$, Q_p corresponding to the peak position [the Debye relation in Eq. (1)]. Its width will be indicative of the correlation range of the associated Fourier components.³⁰

In SiO₂ we have $d(\text{Si-O})=1.62 \text{ \AA}$, $d(\text{O-O})=2.65 \text{ \AA}$, and $d(\text{Si-Si})=3.12 \text{ \AA}$ (Refs. 25 and 28). None of these distances yields $Q \approx 1.5 \text{ \AA}^{-1}$, when using the approximate reciprocal relation $2\pi/Q_p \approx d$. Moss²⁹ pointed out that $Q_p \approx 1.5 \text{ \AA}^{-1}$ has large contributions from $d(\text{Si-Si}_{2nd})$, $d(\text{Si-O}_{2nd})$, and $d(\text{O-O}_{2nd})$ (Fig. 1, inset), suggesting that this is a feature

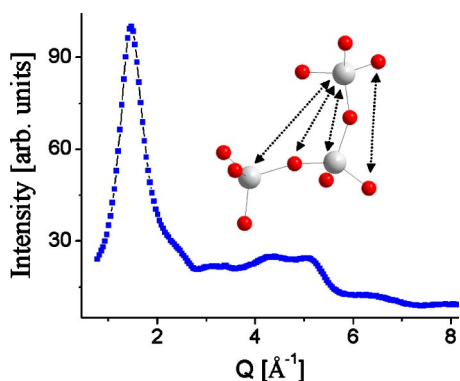


FIG. 1. (Color online) X-ray scattering from vitreous SiO_2 at a laboratory source. Inset: SiO_2 structural units indicating distances that contribute to the FSDP, including the intertetrahedral Si-O-Si distance, which defines the bond-angle. The small dark spheres are oxygen (red); the larger spheres are silicon (white).

related to the way in which the SiO_4 tetrahedra link together (Elliott³⁵ attributes the FSDP to correlations involving network interstitial voids, but this is, by the Babinet principle, an essentially identical statement). Thus such a diffraction feature represents the buildup of correlations whose period is well beyond the first few nearest neighbors. This can probably be better appreciated by using the Debye scattering equation,³⁶

$$I(Q) = \sum_m \sum_n f_m f_n \frac{\sin Qr_{mn}}{Qr_{mn}}. \quad (1)$$

For x rays, $\sin(Qr_{mn})/Qr_{mn}$ are the partial structure factors, and f_m is the atomic form factor for atomic species m (analogously for n). Given Eq. (1), the FSDP actually appears at the maximum of the partial structure factor, i.e., $Q_p = 2\pi(0.715)/d$.

The contribution of the three neutron partial structure factors (Si-Si, Si-O, O-O) to the FSDP was discussed by Robertson and Moss²⁷ using a computer-relaxed Bell and Dean (BD) model.²¹ They paid particular attention to the partial structure factors of the Si-O (which is actually negative), O-O, and Si-Si pair correlations. From those partial structure factors, it appeared that the FSDP was present in all three partial structure factors, indicating that not only the Si-Si partial (associated with intertetrahedral correlations) reflected a contribution. The relaxation of the BD model led to a mean angle $\theta(\text{Si-O-Si}) = 148.7^\circ$, with a much narrower spread $\approx 10^\circ$, a value close to that given in a very recent study of amorphous germania and silica.²⁵

In a variety of different amorphous materials, the connectivity of the constituent structural units may vary, yet an interference is expected to arise from those units in CRN glasses.³⁰ Of course, one cannot simply infer the structure of amorphous materials from the FSDP; nevertheless, the random packing of these units can provide a convenient way to extract the relationship between MRO and SRO correlations.³⁰

In this paper we show how the typical isotropy of the FSDP, present in amorphous bulk SiO_2 , is altered by the

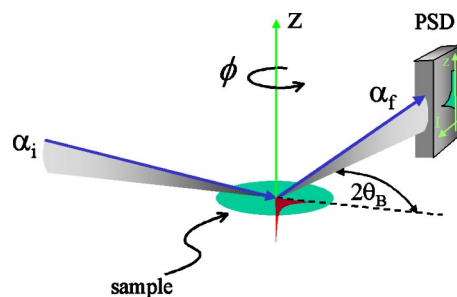


FIG. 2. (Color online) Grazing-incidence diffraction (GID) geometry using a position-sensitive detector (PSD). Shown also is the exponential decay of the evanescent wave. θ_B is the angle corresponding to the in-plane position of interest.

$\text{Si}(001)$ template, turning into a fourfold feature (in Q space and intensity when the sample is rotated about the $\text{Si}\langle 001 \rangle$ normal), of a rather specific kind in relation to the substrate.

III. MATERIALS AND METHODS

The thin film samples under investigation were prepared at North Carolina State University with an RCA cleaning that leaves a thin native oxide on p -type $\text{Si}(001)$ -oriented high-quality wafers from Okmetic, which showed $\approx 0.2^\circ$ miscut at $\approx 5^\circ$ off the $\langle 100 \rangle$ (this vicinality cannot, however, induce a fourfold modulation in the glass). The cleaned samples were then loaded into a tube furnace for thermal oxidation at 1123 K for 30 min and 1223 K for 66 min to produce 100 and 500 \AA SiO_2 films (determined by ellipsometry), respectively.

In an experiment performed on beam line X22C at the National Synchrotron Light Source (NSLS) we used x-ray radiation at 11 keV ($\lambda = 1.1271 \text{ \AA}$), in a bisecting reflectivity mode, to determine the thickness, roughness, and electron density profile of the 100 \AA SiO_2 film. This sample was mounted within a cylindrical beryllium (Be) dome, which was filled with helium (He) gas. The purpose of the He atmosphere was to improve the signal-to-background ratio and to prevent any contamination of the film. It was possible to cover a perpendicular momentum transfer range $Q=0 \rightarrow 0.77 \text{ \AA}^{-1}$ with the detector effectively integrating over the exit angle, α_f , and thus over depth, as we shall describe below. Additionally, grazing-incidence measurements (Fig. 2) in radial and azimuthal modes of the $\text{Si}(2\ 2\ 0)$ yielded information about stress in the sample.

The various experimental sessions at the Advanced Photon Source (APS), beamline 4-ID-D, had basically a similar experimental setup. There were, however, variations in the sample environment, the thickness of the sample, and the x-ray wavelength; those changes will be indicated when we discuss the results.

In the first APS experiment an energy of 20 keV was used ($\lambda = 0.6199 \text{ \AA}$). The sample, 100 \AA SiO_2/Si , was placed inside a Be can filled with He (as earlier done at X22C). At the working wavelength, the critical angle for total external reflection was $\alpha_c = 0.087^\circ$.

The 100 \AA sample was vertically aligned, and a slit oriented normal to its surface was vertically open, to allow all

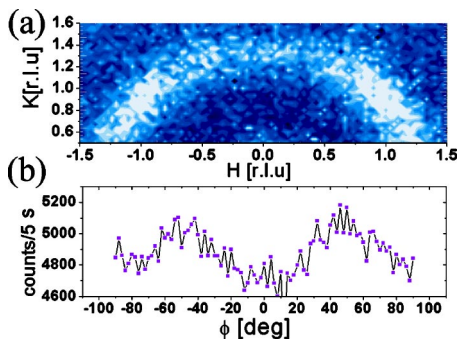


FIG. 3. (Color online) 100 Å SiO₂ film: (a) $HK0$ map in the Si crystal notation. The FSDP modulation can be observed to peak in the Si[1 1 0] directions. (b) ϕ scan of the FSDP position, roughly corresponding to the Si(1 1 0) position. No thermal diffuse streaks were observed in this region.

scattered photons into a scintillation detector. With this configuration α_f was not restricted and the entire SiO₂ film thickness could be probed. With the x-ray beam at an incident angle α_i (see Fig. 2), of 0.05°, i.e., below the critical angle, an $HK0$ map in reciprocal space [Fig. 3(a)] was obtained [$H=-1.5 \rightarrow 1.5$ reciprocal lattice units (r.l.u.), $K=0.5 \rightarrow 1.6$ r.l.u., and $L=0$ r.l.u.]. This reciprocal space map covers the Si(1 1 0) and Si($\bar{1}$ $\bar{1}$ 0) positions (1.636 Å⁻¹), which are Bragg reflections forbidden by symmetry in the bulk Si. Also the bulk glass FSDP position (1.5 Å⁻¹) is enclosed in this area. Thus we were able to explore the azimuthal dependence of the amorphous scattering factor.

An independent measurement that consisted solely in rotating the sample about its normal, Fig. 3(b), traced only the radius corresponding to Si(1 1 0). It shows the FSDP amplitude modulation as observed in the $HK0$ map. Investigation of $\lambda/2$ contamination using attenuators showed no contribution to the enhanced intensity observed in the Si[1 1 0] directions.

To investigate the depth dependence and to understand the nature of the transition layer in more detail, a sample of 500 Å SiO₂ was analyzed, using 10 keV x rays ($\lambda=1.239$ Å). The sample was placed inside a cryostat at 10 K to suppress any bulk Si crystal thermal diffuse scattering (TDS) contribution. The use of the cryostat restricted us to mounting the sample in the horizontal position (the vertical polarization of the x-ray beam is $P=1$, while horizontally $P=\cos^2 \theta$; θ is the scattering angle.), which entailed polarization corrections during the data reduction. Prior to placing the sample inside the cryostat, it was cleaned with acetone for 5 min, followed by ethanol for 5 min; the ethanol was then rinsed with deionized water. A last step of the cleaning process included flowing nitrogen to dry the sample surface. This cleaning process has the overall intention of removing possible organic contamination,³⁷ observed in the 100 Å film (a contamination that, as noted later in the discussion, did not affect our principal results). The scattered photons were collected with a position-sensitive detector (PSD), oriented perpendicular to the sample surface, as in Fig. 2. This detector is capable of simultaneously registering photons along a 50 mm window and thus recording intensity as function of α_f . Photons scattering from different sample depths can thereby be accounted

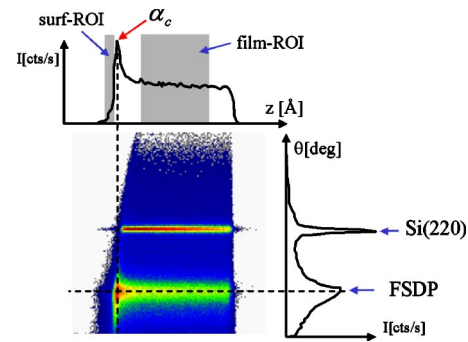


FIG. 4. (Color online) Contour plot of a PSD data set. Dashed lines indicate the position of the cross sections. Top projection: critical angle α_c , and surface and film ROI are indicated. Right-hand side projection: Si(220), and FSDP positions. The FSDP as a function of ϕ was obtained for each radial scan.

for. A slit is also set perpendicular to the sample (Fig. 2) to define the resolution in 2θ . This geometry gave the 100 μm PSD resolution an angular step size of 0.004° in the final angle, α_f . α_f was recorded between between 0.176° below and 0.848° above the critical angle, $\alpha_c=0.174^\circ$. Two different incident angles, α_i , were used: 0.15° and 0.25°.

Series of PSD data sets were collected. Each PSD set was separated into two regions of interest (ROI): one below the critical angle (where the intensity versus α_f peaks), and another above the critical angle, α_c . The ROI below the α_c is mostly surface sensitive (surface ROI), while the ROI above α_c includes information down to the bulk (film ROI), i.e., from the entire film; this is indicated in Fig. 4. In the particular PSD scan of Fig. 4 the Si(220) reflection and the FSDP position can be observed.

Successive radial scans, using the PSD detector, with the sample rotated about its normal at intervals of 10°, collected surface and bulk information within a 180° range. Scattering depths between 40 and 130 Å can be explored with $\alpha_i=0.15^\circ$, while the scattering depths for $\alpha_i=0.25^\circ$ range from 60 to 8000 Å (Refs. 38 and 39).

Our last experiment on thin SiO₂ was carried out at the ESRF, beamline ID1. The scattering was done horizontally, due to technical constraints. The scattered photons of energy 7.2 keV ($\lambda=1.722$ Å) were collected by a PSD vertically oriented respect to the sample surface (Fig. 2). At this energy the critical angle was, $\alpha_c=0.2421^\circ$. The 500 Å SiO₂ film sample was placed inside a kapton cone filled with helium to reduce air scattering.

We registered data at two different incident angles ($\alpha_i=0.15^\circ, 0.30^\circ$), through a series of ϕ scans, at different radii (Q_{\parallel}) in reciprocal space; this scan was achieved by moving the diffractometer detector arm to the appropriate angular position (in a $4S+2D$ diffractometer). Q_{\parallel} was thus scanned between 0.4455 Å⁻¹ and 3.0840 Å⁻¹, while ϕ covered a range of 180°.

As was done in the APS experiments while using the PSD, a surface ROI and a film ROI were identified, in order to extract the FSDP depthdependence. With the available setup the final angle varied 0.17° (≈ 4 mrad) below α_c , and 1.125° (≈ 22 mrad) above α_c . Scattering depths between 35 and 80 Å were explored with $\alpha_i=0.15^\circ$ and between 60 and 5000 Å with $\alpha_i=0.30^\circ$.

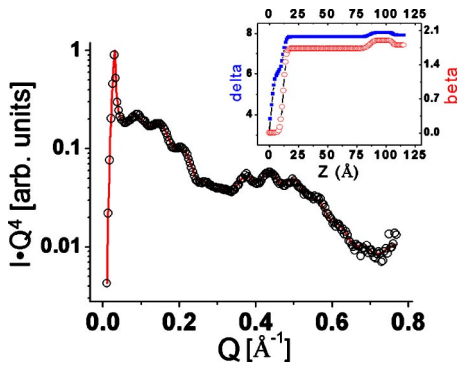


FIG. 5. (Color online) 100 Å SiO₂ reflectivity curve, Fresnel normalized; the line is the fit; and open circles are data. Inset: Calculated electron density (\approx delta, in units of 10^{-6} ; squares), and absorption (\approx beta, in units of 10^{-7} ; open circles); surface at $z=0$.

IV. RESULTS AND DISCUSSION

From reflectivity measurements at $\lambda=1.1271$ Å that covered a range of $Q=0\rightarrow 0.77$ Å⁻¹, Fig. 5, we observed a series of oscillations that were enhanced by Fresnel normalization.⁴⁰ The Fresnel reflectivity has a Q^{-4} dependence, which is a factor included in the actual measured reflectivity, the other factor being that part of the reflectivity that departs from a system with perfectly flat interfaces between the media composing the sample. By multiplying by Q^4 , we are more sensitive (the fit can be more accurate) to the second factor and thus to properties of the sample.

Figure 5 includes as well the fit (red line), the experimental data (open circles), and the inset contains the model, i.e., the $\delta(\lambda^2 N r_0 Z / 2\pi)$ and $\beta(\lambda N \sigma_0 / 4\pi)$ parameters (λ is the wavelength, N the electron density, r_0 the Thompson scattering length, and σ_0 the absorption coefficient); δ and β are associated with the complex refractive index, $n=1-\delta i\beta$. The sample is modeled to be composed of strata and a substrate. The three strata included in the model have different electron densities, absorptions, thicknesses, and roughnesses, values that were calculated applying the Parrat⁴¹ formalism, using a least-squares minimization method.

An uppermost layer, of 12 Å, was identified, and considered to be due to organic material,³⁷ denatured by the x-ray radiation, but otherwise of no interest in this study. The most prominent oscillation period corresponds to 74 Å and represents amorphous SiO₂. At the interface, a layer of ≈ 20 Å was found, with a rms roughness of ≈ 5 Å between interface and substrate. The inset in Fig. 5 shows the thickness variation of δ and β . The film surface is located on the left-hand side ($z=0$). In the profile, a lower electron density (the absorption decays more abruptly; red circles) is located at the surface, and a 3% (compared to the 74 Å layer) enhanced electron density layer is observed at the interface. The substrate is on the extreme right of the inset. The rapid decrease of the absorption factor, β , indicates that it is composed of a material with low absorption—hence the contamination—while δ decays more gradually as it is due to scattering.

Figure 6 shows the results of our grazing-incidence diffraction (GID) scan through the Si(2 2 0), at $\alpha_i=0.2^\circ$. There

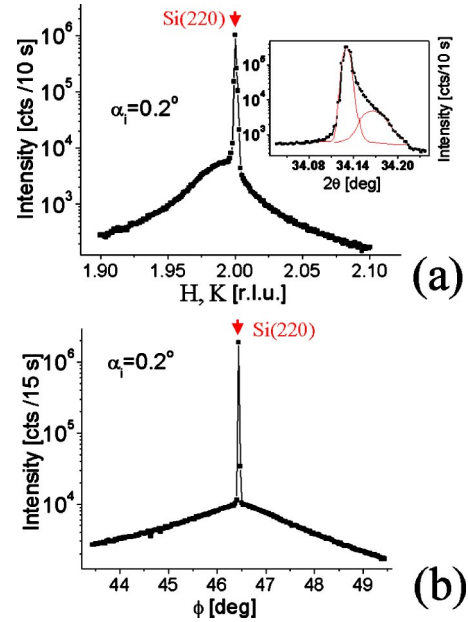


FIG. 6. (Color online) 100 Å grazing incidence profiles at $\alpha_i=0.2^\circ$ (above the critical angle $\alpha_c=0.15^\circ$) and $\lambda=1.1271$ Å. The Si(2 2 0) position is highlighted with an arrow. (a) Radial scan through Si(2 2 0); the inset is a close-up of this Si(2 2 0), where a dilation of the Si lattice parameter is observed in the stronger peak, leading to a compression normal to the film; two Gaussians were added to guide the eye. (b) azimuthal scan through Si(2 2 0). In both profiles, neglecting the inset, there is a broad feature perhaps due to the oxygen incorporation into the silicon, although in (a) it does not follow a Q^2 law, typical for point defects (Ref. 46). The full width at half maximum of the broad feature is ≈ 0.034 r.l.u. in the radial scan, ≈ 0.008 r.l.u. away from the Si(2 2 0) (b), and $\approx 2.45^\circ$ in the azimuthal scan (a), this last breadth translates into a correlation range of ≈ 250 Å.

is a clear broad peak with a maximum slightly displaced to a lower angle which we tentatively associate with a crystalline component discussed in the following paper⁵² (paper II). The inset of Fig. 6(a) shows solely the Si(2 2 0) (giving a $1/e$ penetration of ≈ 80 Å at the incident angle used), with a shoulder extending toward a higher angle ($\Delta 2\theta \approx 0.035^\circ$). Because of the evanescent nature of the wave field, we attribute the stronger peak to the interfacial Si and the shoulder to the bulk. This indicates an interfacial compression normal to the film surface. The asymmetry of the profile gives a strain $\epsilon \approx 1 \times 10^{-3}$, comparable with an estimation of the thermal mismatch strain $\epsilon \approx 1.7 \times 10^{-3}$ [calculated from $\epsilon = (\alpha_{T(\text{SiO}_2)} - \alpha_{T(\text{Si})})\Delta T$; $\alpha_{T(\text{SiO}_2)} = 2.6 \times 10^{-6} \text{ K}^{-1}$ (Ref. 42), $\alpha_{T(\text{Si})} = 0.5 \times 10^{-6} \text{ K}^{-1}$ (Ref. 43), and ΔT is the temperature variation between oxide formation and room temperature]. Some distortion in the Si close to the interface¹¹ follows from the previous discussion, which will carry a densification of Si, normal to the film, and thus account for part of the 20 Å interfacial layer, noted in the reflectivity curve of Fig. 5. The broad component in Fig. 6(b) is related to the shape transform of the crystalline phase discussed in the following paper⁵² (paper II). This rather unusual line shape is observed transverse to the radial scan, which, when plotted on a linear scale shows a correlation length of ≈ 250 Å. The expectation

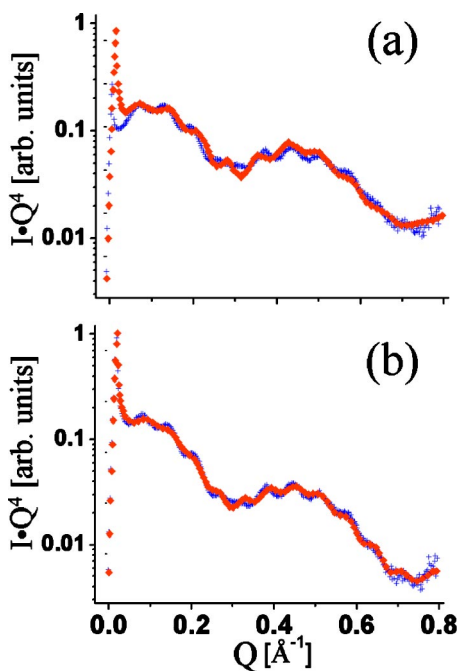


FIG. 7. (Color online) Reflectivity of 100 Å SiO₂ film. Fit (two layers and a substrate, red diamonds); and experiment (blue crosses): (a) fit with only two layers, (b) best fit with two layers. Clearly, the interface in Fig. 5 is required for the best fit.

is that this corresponds to the form factor of the crystallites, revealing a structure with a larger cross section near the interface and smaller towards the thin film surface (see paper II). The shape (semitriangular on a logarithmic scale) is currently being analyzed in a manner similar to the work of Kegel *et al.*^{44,45} but without their consideration of concentration.

Figures 7(a) and 7(b) are included for a clearer understanding of the reflectivity fitting process. The two fits correspond to a model with *only* two layers: a very superficial one followed, towards the substrate, by an SiO₂ layer (and of course a substrate, crystalline silicon). Figure 7(a) corresponds to a relatively “bad” representation of the experimental findings. Our best attempts to improve the fit, using *only* two layers, yielded the curve in Fig. 7(b). In both cases it is fairly clear to the eye, that there is a phase shift, most noticeably between $Q=0.05$ and $Q=0.25$ Å⁻¹. The phase shift is the strongest indicator of the need to include a third layer in the model, as shown in Fig. 5.

Another portion of the analysis here presented consists of quantifying the FSDP intensity and position variations. In Fig. 3(a) a semiring can be observed. The semiring corresponds to the FSDP position in the reciprocal space *HK0* map, its maximum expanding to 1.636 Å⁻¹ at the Si(1 1 0) positions. Not only a radial expansion occurs, but also the intensity varies, gradually decaying by 200 counts along the semiring and away from the Si(1 1 0) positions. As the intensity decays, the semiring reduces its radius, relative to the origin, to 1.4 Å⁻¹. This leaves some ambiguity resulting from the variation in Fig. 3(b), which is due to both the varying intensity and the radial position.

The integrated PSD data obtained from the 500 Å film in Fig. 8(a) clearly display the fourfold modulation of the

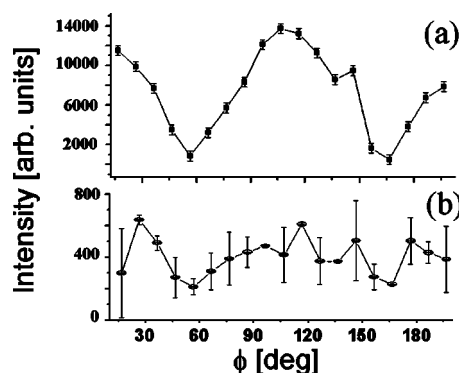


FIG. 8. FSDP values for the 500 Å film at their corresponding ϕ positions: (a) down to the interface with bulk Si, film ROI, and (b) within the topmost 100 Å, surface ROI. Clearly the surface ROI shows essentially no anisotropy, while the film ROI does.

FSDP. The peak about $\phi=110^\circ$, Fig. 8(a), corresponds to the Si($\bar{1}$ 1 0) direction, while about $\phi=20^\circ$ the Si(1 1 0) is located. Although the scan along Si($\bar{1}$ 1 0) was not completed, due to technical limitations of the diffractometer, the trend of the intensity increase is still present, similar to the 100 Å film in Fig. 3. Here, however, the peak is determined using radial scans in 10° intervals and then plotting its maximum at Q_p . In this case, the FSDP shifts to 1.485 Å⁻¹ at the position of maximum intensity and to 1.455 Å⁻¹ at the minimum; the difference between these two values is smaller than in the 100 Å film, but the positions are consistently different, in reciprocal space, from the 1.5 Å⁻¹ FSDP value typical of the bulk. On the other hand, the profile corresponding to the surface region, Fig. 8(b), has a statistically null FSDP modulation. For $\alpha_i=0.15^\circ$ the data yielded qualitatively analogous results but with lower counting statistics (not shown).

Figure 9 shows the azimuthal dependence, in the ESRF data, of the FSDP for $\alpha_i=0.3^\circ$ film ROI and surface ROI at 1.722 Å. There are again two prominent peaks [Fig. 9(a)] at about $\phi=-75^\circ$ and 15° , which correspond to the Si($\bar{1}$ 1 0) and Si(1 1 0) directions, respectively. The counting statistics of the surface-ROI ϕ scan in Fig. 9(b) exhibits essentially no FSDP modulation.

Figure 10 represents another view of the collected data. *HK0* maps indicate the Si($\bar{1}$ 1 0) and Si(1 1 0) directions. In

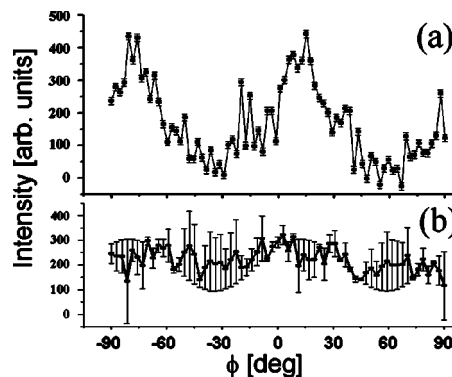


FIG. 9. ESRF ϕ scans on the 500 Å film about the FSDP position for $\alpha_i=0.3^\circ$; (a) surface ROI, (b) film ROI. Clearly the modulation in the surface ROI is statistically absent.

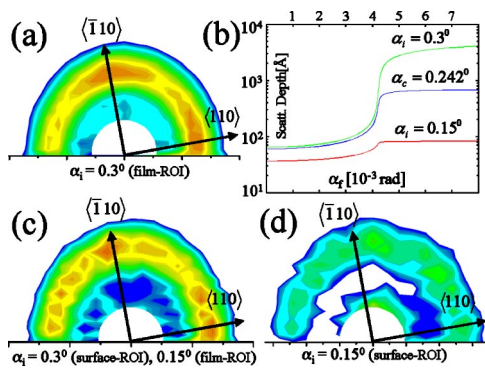


FIG. 10. (Color online) $HK0$ maps of 500 Å film (a), (c), and (d). (b) Scattering depths for the working angles $\alpha_i = 0.3^\circ$ and 0.15° .

Fig. 10(a) the fourfold modulation is clear. A modulation can barely be observed in Fig. 10(c); this figure basically has the same appearance for both $\alpha_i = 0.3^\circ$ and 0.15° , in their respective surface- and bulk-ROI representations. This last is not entirely surprising judging by the scattering depth curves shown in Fig. 10(b). In Fig. 10(d) the FSDP modulation is absent.

A prominent feature of the amorphous SiO_2 is the FSDP,^{27,29,30,32–35} to which we have devoted significant attention. Useful structural correlations are associated with it, generally referred to as intermediate-range order, which include distances well beyond the first-nearest Si-O neighbors in the Fig. 1 inset. The FSDP is thus clearly related to the degree of order among the interconnected SiO_4 tetrahedra in the film.

Coincidence of the FSDP with the $\text{Si}(1\ 1\ 0)$ positions assisted us in scaling the degree of structural compression of the tetrahedral units. There is a compression variation of about 8% along $[1\ 1\ 0]$ in the 100 Å film while the 500 Å film registers a smaller variation, about 2%. Both variations are compared to the standard vitreous silica FSDP. Earlier measurements of the refractive index of SiO_2 (Refs. 47 and 48) showed a negative slope as a function of growth temperature, which should be attributed to relaxation in the structural components of the glass. Thinner films are grown at lower temperatures, at which higher compression would induce higher electron density, that being the reason for a larger compression variation in the 100 Å film. Pressure changes in the glass have been considered in the past^{35,49,50} as responsible for FSDP intensity variations. The difference in the interfacial strain found in the reflectivity and in the variation in the FSDP is due to the fact that the reflectivity normal to the surface averages the lateral compressive and tensile components in the glass as it forms.

The experiments at 7.2 keV, at the ESRF, basically confirm those obtained with a higher energy, 10 keV at the APS. Measurements in both cases were carried out on 500 Å samples. Although preferential orientation along $\text{Si}[1\ 1\ 0]$ has been stressed, as being responsible for the structure factor modulation, we have to note as well that this is strongest close to the substrate. Judging by the low counting statistics (Fig. 9) in the surface sensitive depth-dependence investigations (within 80 and 35 Å depth, depending on α_i), there is a vanishingly small preferential orientation along $\text{Si}[1\ 1\ 0]$ close to the surface.

In summary, since we are interested in discussing the structure of these amorphous SiO_2 films, it is convenient to consider the variations in the type of connections between coordination polyhedra in the glass. Those variations in the packing connectivity, which occur anisotropically in the thin film, aided by the $\text{Si}(001)$ symmetry, are responsible for the enhanced electron density observed in the reflectivity measurements, Fig. 5, together with the FSDP enhanced intensity and its positional variation along the $\text{Si}[1\ 1\ 0]$. We note here that Reichert *et al.*,⁵¹ studying liquid Pb over $\text{Si}(001)$, found both a fourfold modulation (as did we), as well as strong evidence for fivefold icosahedral fragments of the liquid layers captured by the Si crystal.

Together with the experiments described in the present work, crystal truncation rod data along $\text{Si}(1\ 1\ L)$ disclose the presence of a crystalline peak accompanied by Laue oscillations. The significance of those results, their relation to Fig. 6, and a model proposed to explain them, will be discussed in more detail in the following paper, paper II.⁵²

The present results help to complement the understanding of the oxidation process in silicon. Subsequent models must include a mechanism that permits ordered regions to coexist within the amorphous matrix, without causing cracks or defects that destroy the gate oxide. The modulated glass results from this requirement.

ACKNOWLEDGMENTS

We would like to acknowledge the assistance of H. Zajonz (X22C, NSLS) and J. C. Lang (4-ID-D, APS). This work was supported by the Department of Energy (DOE) under Contract No. DE-FG03-01ER45880. Use of the APS was supported by the U.S. DOE, Office of Science, Office of Basic Energy Sciences, under Contract No. W-31-109-Eng-38. Research carried at the NSLS, BNL, was supported by the U.S. DOE, Division of Materials Sciences and Division of Chemical Sciences, under Contract No. DE-AC02-98CH10886.

¹C. J. Sofield and A. M. Stoneham, *Semicond. Sci. Technol.* **10**, 215 (1995).

²R. M. Wallace and G. Wilk, *MRS Bull.* **27**, 192 (2002).

³E. P. Gusev, H. C. Lu, T. Gustafsson, E. Garfunkel, *Phys. Rev. B* **52**, 1759 (1995).

⁴D. A. Muller, T. Sorsch, S. Moccio, F. H. Baumann, E. Evans-

Lutterodt, and G. Timp, *Nature (London)* **399**, 758 (1999).

⁵K. Hirose, H. Nohira, T. Koike, K. Sakano, and T. Hattori, *Phys. Rev. B* **59**, 5617 (1999).

⁶C. Westphal, *Appl. Phys. A: Mater. Sci. Process.* **76**, 721 (2003).

⁷A. Ourmazd, D. W. Taylor, J. A. Rentschler, and J. Bevk, *Phys. Rev. Lett.* **59**, 213 (1987).

- ⁸A. Pasquarello, M. S. Hybertsen, and R. Car, *Phys. Rev. Lett.* **74**, 1024 (1999).
- ⁹A. Demkov and O. F. Sankey, *Phys. Rev. Lett.* **83**, 2038 (1999).
- ¹⁰Y. Tu and J. Tersoff, *Phys. Rev. Lett.* **89**, 086102 (2002).
- ¹¹A. Bongiorno, A. Pasquarello, M. S. Hybertsen, L. C. Feldman, *Phys. Rev. Lett.* **90**, 186101 (2003).
- ¹²K. Tatsumura, T. Watanabe, D. Yamasaki, T. Shimura, M. Umeno, and I. Ohdomari, *Phys. Rev. B* **69**, 085212 (2004).
- ¹³A. C. Wright, *J. Non-Cryst. Solids* **179**, 84 (1994).
- ¹⁴M. H. Cohen and G. S. Grest, *Phys. Rev. B* **20**, 1077 (1979).
- ¹⁵L. G. Van Uiter, *J. Appl. Phys.* **50**, 8052 (1979).
- ¹⁶F. H. Stillinger, *Science* **267** 1935 (1995).
- ¹⁷X. Xia and P. G. Wolynes, *Phys. Rev. Lett.* **86** 5526 (2001).
- ¹⁸R. W. Hall and P. G. Wolynes, *Phys. Rev. Lett.* **90** 085505 (2003).
- ¹⁹Z. P. Lu and C. T. Liu, *Phys. Rev. Lett.* **91** 115505 (2003).
- ²⁰R. L. Mozzi and B. E. Warren, *J. Appl. Crystallogr.* **2**, 164 (1969).
- ²¹R. J. Bell and P. Dean, *Philos. Mag.* **25**, 1381 (1972).
- ²²L. F. Gladden, T. F. Carpenter, and S. R. Elliott, *Philos. Mag. B* **53**, L81 (1986).
- ²³R. F. Pettifer, R. Dupree, I. Farnan, and U. Sternberg, *J. Non-Cryst. Solids* **106**, 408 (1988).
- ²⁴P. Vashishta, R. K. Kalia, J. P. Rino, and I. Ebbsjö, *Phys. Rev. B* **41**, 12197 (1990).
- ²⁵J. Neufeind and K. D. Liss, *Ber. Bunsenges. Phys. Chem.* **100**, 1341 (1996). We believe this to be the most definitive of the studies, especially with regard to the measured bond angle distribution.
- ²⁶S. R. Elliott, *Physics of Amorphous Materials* (Longman, London, 1983).
- ²⁷J. L. Robertson and S. C. Moss, *J. Non-Cryst. Solids* **106**, 330 (1988).
- ²⁸D. A. Keen and M. Dove, *J. Phys.: Condens. Matter* **11**, 9263 (1999).
- ²⁹S. C. Moss, in *Amorphous and Liquid Semiconductors*, edited by J. Stuke and W. Brening (Taylor and Francis, London, 1973), p. 17.
- ³⁰S. C. Moss and D. L. Price, in *Physics of Disordered Materials*, edited by D. Adler, H. Fritzsche, and S. R. Ovshinsky (Plenum Press, New York, 1985), p. 77.
- ³¹S. R. Elliott, *Phys. Rev. Lett.* **67**, 711 (1991).
- ³²J. Swenson and L. Borgesson, *J. Non-Cryst. Solids* **223**, 223 (1998).
- ³³C. Z. Tan and J. Arndt, *J. Non-Cryst. Solids* **249**, 47 (1999).
- ³⁴C. Massobrio and A. Pasquarello, *J. Chem. Phys.* **114**, 7976 (2001).
- ³⁵S. R. Elliott, *Nature (London)* **354** 445 (1991).
- ³⁶B. E. Warren, *X-Ray Diffraction* (Dover, New York, 1990).
- ³⁷J. A. Dura, C. A. Richter, C. F. Majkrzak, and N. V. Nguyen, *Appl. Phys. Lett.* **73**, 2131 (1998).
- ³⁸H. Dosch, *Phys. Rev. B* **35**, 2137 (1987).
- ³⁹H. Dosch, *Critical Phenomena at Surfaces and Interfaces: Evanescent X-ray and Neutron Scattering*, edited by G. Hoehler (Springer-Verlag, Heidelberg, 1992).
- ⁴⁰S. K. Sinha, E. B. Sirota, S. Garoff, and H. B. Stanley, *Phys. Rev. B* **38**, 2297 (1988).
- ⁴¹L. G. Parrat, *Phys. Rev.* **95**, 359 (1954).
- ⁴²Y. Okada and Y. Tokumaru, *J. Appl. Phys.* **56**, 314 (1984).
- ⁴³*Handbook of Chemistry and Physics*, 37th ed., edited by C. D. Hodgman, R. C. Weast, and S. M. Selby (Chemical Rubber, Cleveland, OH, 1956).
- ⁴⁴I. Kegel, T. H. Metzger, J. Peisl, J. Stangl, G. Bauer, and D. Smilgies, *Phys. Rev. B* **60**, 2516 (1999).
- ⁴⁵I. Kegel, T. H. Metzger, A. Lroke, J. Peisl, J. Stangl, G. Bauer, K. Nordlund, W. V. Shoenfeld, and P. M. Petroff, *Phys. Rev. B* **63**, 035318 (2001).
- ⁴⁶M. Sztucki, T. H. Metzger, I. Kegel, A. Tilke, J. L. Rouvière, D. Lübbert, J. Arthur, and J. R. Patel, *J. Appl. Phys.* **92** 3694 (2002).
- ⁴⁷A. G. Revesz, B. J. Mrstik, and H. L. Hughes, in *The Physics and Technology of Amorphous SiO₂*, edited by R. A. B. Devine (Plenum Press, New York, 1987), p. 299.
- ⁴⁸A. Szekeres, K. Christova, and A. Paneva, *Philos. Mag. B* **65**, 961 (1992).
- ⁴⁹S. Tanaka, *J. Non-Cryst. Solids* **90**, 363 (1987).
- ⁵⁰C. Meade, R. J. Hemley, and H. K. Mao, *Phys. Rev. Lett.* **69**, 1387 (1992).
- ⁵¹H. Reichert, O. Klein, H. Dosch, M. Denk, V. Honkimaki, T. Lippmann, and G. Reiter, *Nature (London)* **408**, 839 (2000).
- ⁵²M. Castro-Colin, W. Donner, S. C. Moss, Z. Islam, S. K. Sinha, and R. Nemanich, following paper, *Phys. Rev. B* **71**, 045311 (2004).